THE COMPARISON BETWEEN THE DYNAMIC STALL OF A FINITE WING WITH STRAIGHT AND SWEPT TIPS

R.A.McD. Galbraith, F.N. Coton, D.Jiang, R. Gilmour

Department of Aerospace Engineering, The University of Glasgow, Glasgow, G12 8QQ, U.K.

Abstract

This paper presents results from a new facility specifically designed to measure the static pressure distributions over finite wings undergoing arbitrary pitching motions through dynamic stall. The two sets of data presented are for a rectangular planform wing and a similar span and chord model but with swept tips both instrumented with 192 miniature pressure transducers. Apart from describing the test facility, typical data from a high speed ramp-up motion to beyond stall are discussed. The data illustrate the three-dimensionality of the flow, including the manner in which, on both wings, the tip vortices influence the development and subsequent convection of the dynamic stall vortex. The differences in the behaviour of the vortex systems on the two wings are discussed and qualitative flow models are proposed.

Nomenclature

c	chord
Cn	normal force coefficient
Cp	pressure coefficient
r	reduced pitch rate $\left(\dot{\alpha}c/2U\right)$
Re	Chord Reynolds number
s	span
x	chordwise direction
y	direction normal to chord
z	spanwise direction
U	velocity
α	angle of attack
ω	rotational velocity

Introduction

It has been recognised for many years[1] that the maximum lifting force generated by a wing can be substantially enhanced if the wing is subject to rapid pitching motion. The detailed mechanisms which interact to produce this 'dynamic-stall' effect, however, are still not fully understood despite being of significance to both rotary-wing and fighter aircraft. This is, in part, because of the difficulties in accurately measuring and interpreting features of a strongly three-dimensional flow field. For this reason, almost all the early dynamic-stall tests were performed under nominally two-dimensional flow conditions. Even then, however, early studies[2] clearly showed that, although the flow was nominally two-dimensional for the fully attached steady flow case, the stall cells were highly three-dimensional.

The perceived need to have a better insight into the phenomena associated with dynamic stall encouraged many more experimenters to design and develop their own research facilities. Of particular note are the works of McCroskey et al.[3], McAllister et al.[4], Petot [5], Wood[6] and Carta et al.[7] which, although focusing on the two-dimensional problem, provided valuable insight into the dominant flow mechanisms. In fact, on the basis of these works and several others, Young[8] was able to propose a good description of the characteristic phenomena associated with dynamic stall. A further notable review of progress in the field was later provided by Carr[9].

Although Young's description has been generally accepted as a fair assessment, the totality of the process is still poorly understood. For example, two seemingly equivalent experiments (Lorber & Carta[10], Galbraith et al.[11]), pertaining to the effect of pitch rate on the convection velocity of the dynamic stall vortex, have yielded contradictory results . Green and Galbraith [12], who spent much effort assessing both the data sets involved, concluded that, if the geometric environment of the experiments was similar, the difference was most likely associated with the respective Mach numbers; 0.17 and 0.3.

Albeit there were anomalies to be reconciled and a better understanding of the effect of Mach number, Reynolds number and tunnel environment required, the data have been put to good use in the development of semi-empirical dynamic stall models such as those of Beddoes[13], Lieshman & Beddoes[14], Gangwani[15] and Tran & Petot[16]. Such models are predominantly two-dimensional and, although, as demonstrated by

Beddoes[17], they can be coupled to an appropriate wake model to cope with the three-dimensional planform in the region of a helicopter blade tip, there are very little data and detailed understanding with which to test and develop those preliminary attempts.

The tip region of helicopter blades has been further complicated by the emergence of new planforms including the so-called BERP tip. These tips can have highly swept leading edges which may produce fundamental differences between the stalling pattern at the tip and over the larger part of the rotor. The swept tip may be dominated, on the retreating side of the rotor disc, by a strong vortex similar to that of a delta wing, whilst the inner portions may be more akin to the two-dimensional test case. Thus, useful information on the complexities of the stall process may be obtained by isolating the differences between the dynamic stalling of a finite straight wing and that of a delta wing, and examining to what extent both associated phenomena interact for a straight wing with highly swept tips.

Improved understanding of these phenomena require the execution of three-dimensional dynamic stall experiments of which, to date, there are but a few. Of these, the majority have been motivated by aspects of fighter aircraft manoeuvrability and have thus considered only delta wings[18,19]. A small number of tests have, however, been carried out on other wing planforms using a range of measurement techniques. In studies at the University of Colorado, flow visualisation, surface pressure measurement and hot wire anemometry was used to investigate the flow around oscillating cantilevered wing planforms[20,21]. Some foresighted flow visualisation experiments were carried out at the same institution by Freymuth[22] and later Horner et al.[22] investigating both the manner of the stall and the associated connectivity of vortical structures. A more involved experiment was carried out by Pezali[24] at NASA Ames and involved a cantilevered finite wing heavily instrumented with pressure transducers.

For the past few years the authors have been developing a three-dimensional dynamic-stall facility to provide data on the effects of planform on the dynamic stalling process. To date three finite wings have been tested in the facility; a straight planform[25,26], a delta wing and a straight wing with swept tips at an angle equal to that of the delta wing.

This paper presents a comparison of the stalling characteristics of the straight and swept-tip wings during a rapid "ramp-up" motion. On each model, high frequency pressure measurements were made at 192 surface locations, providing both high temporal and spatial resolution. These data were analysed, together with relevant flow visualisation, to provide qualitative descriptions of the flow structures present in both cases. It was found that, initially, similar vortex structures were produced on both wings, although the manner of their subsequent interaction and convection was quite different.

Description of the Test Facility

The tests were carried out in the University of Glasgow's "Handley Page" wind tunnel which is a low-speed closed-return type. The wing models were located horizontally in its 2.13 × 1.61 metre octagonal working section and supported on three struts, as shown in Fig. 1. These were, in turn, connected to the main support structure and actuation mechanism situated below the tunnel. Movement of the model was produced by displacement of the two rear struts and the model was pivoted about the quarter chord position on a tool steel shaft connected to the front support via two self aligning bearings. The actuation force was produced using a Parker 2H Series linear hydraulic actuator and crank mechanism which allowed a variation of angle of attack from -26^{o} to 45^{o}. This system comprised the 2H series hydraulic cylinder, a bridge manifold, a high response proportional directional control valve with a E200-595 PID analogue closed loop controller and could deliver a maximum thrust of 17KN during extension and 6.53 KN during retraction at a piston speed of 1.1m/s. An angular displacement transducer mounted on the crank was used to provide a feedback signal and for recording the real time angle of attack.

The cross section of both wings was that of a NACA 0015 aerofoil with the tips of the rectangular wing being simple solids of revolution. At the tips of the swept-tip wing, the aerofoil profile shape was retained over approximately the first 15% of the chord and the intersection between the swept edge and the leading edge was rounded. On aft portions, the cross-sectional shape was tapered down to produce sharp leading edges. The overall dimensions of the models were 126 cm x 42cm, giving an overall aspect ratio of 3 for the rectangular wing. Both models were constructed with an aluminium framework of ribs and stringers with an outer epoxy glass fibre skin.

Altogether, 192 pressure transducers were placed within the models predominantly to the starboard side. On the rectangular wing there were six chordal distributions at various spanwise locations, each of which had 30 transducers distributed on both upper and lower surfaces. In the region of the tip, additional transducers were placed between the above mentioned sections to provide a better assessment of the tip vortex movement and structure. On the swept-tip wing, four chordal arrays of 29 transducers were used on the main body of the wing. At the wing tip, a series of swept arrays, emanating from the virtual intersection of the leading edge and swept tip, were employed. The locations of the main transducer arrays on the two models are illustrated in Fig. 2.

In order to check on the overall symmetry of the flow, two transducers were placed on the left side of each wing in corresponding positions to their counterparts on the starboard side. Additionally, three accelerometers were embedded in the wings, two of which were near the trailing edge on outboard locations and the final one was mounted centrally.

All pressure transducers were of Kulite differential type CJQH-187 with one side of the pressure diaphragm open to the ambient pressure outside the wind-tunnel via tubing. The signals from all of the transducers were taken to a specially designed signal conditioning unit of modular construction with each module containing its own control board. On instruction from the computer, the control board automatically removed all offsets to below the A-D converter resolution and adjusted all gains as necessary. In fact, during a test, the computer sampled the maximum and minimum of each transducer output and adjusted the gains accordingly to improve the data acquisition resolution. The data acquisition was carried out by a PC microcomputer, configured with a 486 processor and interfaced with proprietary Bakker Electronics BE256 modules which provided the necessary analogue to digital conversion. The software used for data acquisition was TEAM 256. At present, the system has 200 channels, each of which is capable of sampling to a maximum rate of 50KHz, giving an overall sampling rate of 10MHz.

A high sampling rate was required to capture the fine detail of the dynamic stall process, especially when the reduced pitch rates or reduced frequencies were relatively high. For example, at the reduced frequency of 0.18, where the oscillation frequency at 50 m/sec wind speed is approximately 7Hz, the overall sampling rate was in the region of 30 kHz per channel.

The Test Sequence

For each wing, four particular test motions were considered. The first of these was to assess the steady performance of the wing over an approximate incidence range of -5^{o} to $+40^{o}$. This was carried out at regular intervals as a check on the overall system performance. Second, a sequence of ramp and hold tests, in which the wing was pitched up at a constant rate and then held at approximately 40^{0}, were conducted. For the lower pitch rates, excellent ramp functions were obtained but, as can be imagined, at the higher values the starting and stopping sequences induced non-linearities. Nonetheless, over the area of interest, i.e., stall initiation, the pitch rates remained relatively constant. Third, ramp-down tests in which the wing was exposed to a constant negative pitch rate were carried out and, finally, a series of oscillatory tests more typical of extant dynamic stall experiments were conducted.

Results

As mentioned above, only two of the several hundred test cases recorded will be presented. These have been chosen as being, in the authors' assessment, representative of the dominant dynamic stall flow features observable throughout the "ramp-up" data section. Even within these two selected data sets, the presentations have been restricted to one in every eighty data sweeps. Even so, high quality resolution of the surface pressure distribution is evident.

Figure 3 illustrates the normal force coefficients obtained close to the mid-span or the wing for both models and also their nominal two-dimensional counterpart. The steady data are depicted by the symbols and the obvious dynamic data relate to a non-dimensional pitch rate of 0.027 which, in turn, for the rectangular wing, equates to an actual pitch rate of 411 ^{o}/s. With regard to the static data, the effects of aspect ratio are clearly visible. The nominal two-dimensional test case has the largest lift curve slope whilst the swept tip wing, with the lowest aspect ratio, has the smallest. Under dynamic conditions and in the fully attached state, the two-dimensional test case tends to lag the steady data whilst the two finite wing responses leads the steady state. At the end of the response's linear phase, the two-dimensional data exhibits an increase in gradient (position 1) and a subsequent large peak which is not so evident in either of the finite wings. In fact, at position 2, the rectangular wing appears to be mimicking the characteristics of the two-dimensional data but with the large peak missing; this is even more evident in the swept tip wing.

The corresponding surface pressure histories, associated with these responses, are depicted in Figure 4. It may be seen that, for the rectangular wing, there is a typical increase in suction up to the point of suction collapse. In this region, but not coincidental with it, a pressure wave develops and appears to travel across the chord and becomes indistinct. This is similar to two-dimensional dynamic stall but is far less pronounced than that observed by Galbraith et al [11]. No such clear evidence of pressure waves can be detected for the swept tip wing although, in the region of the mid-chord, there is a discernible bulge in the pressure histories. This is clearly atypical of two-dimensional dynamic stall.

For the rectangular wing, the nominal mid-span (i.e. 57%) location could have been expected to exhibit closest agreement with its two-dimensional counterpart. In Figure 5, which depicts the corresponding normal force coefficients at 66% of span, there is more correspondence of the characteristics there than at the mid-span. For example, it is obvious that the rectangular wing exhibits similar characteristics to the two-dimensional data, although not the same values. In other words, there is a long dynamic overshoot of the steady data followed by a rapid increase in the curve slope and a subsequent peak and rapid decline. There is even evidence of this in the swept tip model. Once again, in the linear phase, the finite wing responses lead the steady data. The corresponding pressure data for this location are given in Figure 6. There, the rectangular wing shows clear evidence of a prominent pressure wave similar to that found in the two-dimensional case and the pressure profile has the hallmark of deep dynamic stall. Even the pressure distributions for the swept case show a more prominent bulge at the stall than at the 57% span. The bulge, however, is not representative of the normal distributions associated with two-dimensional dynamic stall.

Further clues as to the nature of the flow development can be obtained by presenting the span-wise temporal pressure distributions at various chordal locations. For the rectangular wing, these are given in Figure 7 for chord locations of 17, 37 and 83%. As an aid to interpretation, the data from the instrumented half of the wing has been reflected on to the opposite side giving a full span appearance that is symmetric about the mid-span position.

Towards the leading edge of the wing (at 17% chord) the normal expected build up of spanwise pressure is evident until position 1 is reached, whereupon a prominent increase in suction may be observed that progresses from the mid-span outwards. It is significant to note that the initial suction rise collapses before it has penetrated to the tip region. A similar chain of events is observable at the 37% of chord position where, in addition, there is an obvious influence from the tip vortex. The initial rapid increase in suction covers the larger part of the span but once again the central suction collapsed prior to the outboard regions. Following total collapse of all spanwise suction, there follows another similar suction profile that is, in all probability, associated with normal Strouhal type vortex shedding. At the trailing edge (83% of chord) it is clear that the tip vortex has a major influence pressure distribution and, further, that the remnants of the initial flow structure noted above cause the two very prominent suction peaks.

The corresponding pressure plots of the swept tip wing are presented in Figure 8 where, as expected, the most prominent features are associated with the tip vortices. At the leading edge the spanwise pressure profile increases as the incidence increases and so too does the suction from the tip vortices. As indicated on the diagram, a very small spanwise region of rapid increase in suction is evident but is short lived and any secondary effects appear to be dominated by the tip region. At the 37% chord location, little evidence of the peak in mid-span suction exists. And finally, at the trailing edge, apart from the influence of the tip vortices, the pressure profiles are relatively featureless.

To aid the interpretation of these pressure data, additional experiments were carried out on similar wings in a low speed flow visualisation tunnel [Coton and Moir[27]]. A small selection of the photographs taken are presented in Figure 10 and correspond to a reduced pitch rate of 0.08. This is higher than that for the pressure data but was necessary to highlight the dominant flow features. What each of the picture sequences illustrate, although not clear for the rectangular wing, is a view looking down the tunnel on to the upper surface of the wing with the smoke being illuminated from above. For the rectangular wing, a clear, well defined, coherent vortex is evident at t = 0.72. This vortex continues to increase in size as in t = 0.8 where the obvious tip vortex is indicated. Following this, the vortex leaves the surface at the centre span and distorts rapidly into a horseshoe or "omega" [23] vortex.

For the swept-tip wing the outline shape is very clear and at t = .76 there is no evidence of any coherent vortex structure along the span. However, at t = .88 one can see what may be the first signs of a very weak structure on the upper surface. Thereafter, this central structure is limited to a very small portion of the span and is rapidly distorted to obtain the characteristic of a simple bulge, similar to that at t = 1.36 on the rectangular wing but far more restricted.

Discussion

In steady flow, finite wings exhibit a spanwise loading distribution as a consequence of the modification to the onset flow by the downwash from the tip vortex systems. The effect of the downwash, which is strongest near the wing tips, is to reduce the effective incidence across the wing. As may be expected, therefore, the extent of the wing which is subject to this effect depends mainly on the aspect ratio. In fact, for low aspect ratio wings, such as the current test models, almost the entire wing exhibits the hallmarks of the downwash effect. A clear illustration of this is evident in the steady data presented in Figs. 3 and 5 where the gradient of the linear portion of the normal force curve is significantly higher in the nominally two-dimensional case than for the two finite wings. Indeed, the Cn curve for the swept tip wing, which has the lowest effective aspect ratio, exhibits the smallest gradient. An inevitable consequence of this behaviour is the progressive delay of stall as the aspect ratio reduces.

When a finite wing is subject to pitching motion, such as in the present case, the temporal change in loading gives rise to shed vorticity. This is also true in the nominally two-dimensional case where the shed vorticity acts to reduce the effective incidence experienced by the aerofoil. As may be observed in Fig. 3., this has the effect of reducing the Cn produced at a given geometric incidence on the linear portion of the curve. On this basis, it could be anticipated that the vorticity shed from the two finite wings would act in the same manner but, conversely, the dynamic Cn response is observed to lead the static data in both cases. The explanation for this lies not in the shed vorticity effect but, rather, in the temporal development of the tip vortices. As the wings are pitched, the strength of the trailed tip vortices at any instant in time depends on the history of the wing loading. Thus, at a given geometric incidence, downstream segments of the tip vortex structure are weaker than those close to the wing. The integrated effect of this vorticity distribution will, therefore, be less than the corresponding static case where the strength of the tip vortex is effectively constant in the steamwise direction. This is further counpounded by the effect of the shed vorticity as described above and, consequently, the downwash produced at a given geometric incidence during the pitching motion will be weaker than that at the static equivalent. The corresponding higher effective incidence, therefore, accounts for the lead in the dynamic Cn response of the finite wings observed in Figs. 3 and 5. In this context, it is interesting to note that the dynamic Cn

response on both wings is marginally closer to the nominally two-dimensional case at the 57% of span location that at the more outboard section.

Despite the three-dimensional effects described above, it may be observed that all the dynamic Cn curves exhibit a degree of commonalty. It is possible, therefore, that the some of the features of the three-dimensional data may be explained by reference to contemporary understanding of nominally two-dimensional dynamic stall. For example, it is known that the suppression of trailing edge separation during the pitching motion leads to a significant extension of Cn growth beyond the point of static stall. At the reduced pitch rate considered, a strong vortex forms near the quarter chord location and grows in strength before travelling rearwards over the aerofoil. The development of this vortex, termed the dynamic stall vortex, produces a localised area of increased suction on the upper surface of the aerofoil which, in turn, produces the more rapid increase in Cn identified at point 1 in Fig. 3. As the vortex begins to move, the leading edge suction peak collapses and Cn stall occurs. Finally, the vortex convects off the trailing edge and flow resembles the bluff body state with characteristic Strouhal shedding.

Little is known of the extent to which dynamic stall on a three-dimensional wing resembles the above behaviour but valuable insight into this problem has been provided by the notable flow visualisation studies of Freymuth[22] and Horner et al.[23]. Their work, although conducted on a flat plate at much lower Reynolds numbers than the present study, noted that a dynamic stall vortex did indeed form, initially, almost uniformly along most of the span. Subsequently, however, the portion of the vortex at the mid-span lifted off the surface during its downstream convection forming a structure which was termed an 'omega' vortex. An illustration of the general form of this vortex is given in Fig. 11 together with a image taken from the series presented for the pitching rectangular wing in Fig. 9. Clearly, a structure consistent with the 'omega' vortex observed by Horner is present in this case also.

On the basis of these results, it is possible to formulate a scenario for the progression of dynamic stall on the finite wing. Initially, the formation of the dynamic stall vortex is dominated by the spanwise distribution of downwash from the tip vortices. This downwash acts to progressively reduce both the effective incidence and the effective reduced pitch rate as the wing tip is approached. The reduction in the effective reduced pitch rate promotes vortex formation at lower geometric incidence whilst the modification of the effective incidence works in the opposite sense. The net result is that the stall vortex initially develops almost uniformly along the span as may be observed in Fig. 9.

Once formed, the vortex continues to grow giving rise to the increase in suction near the leading edge identified in Figs. 4a and 6a. This, in turn, produces the change in the gradient of the local Cn at position 2 in Figs. 3 and 5. The uniformity of the vortex growth is, however, short lived once trailing edge separation begins on the wing. At this stage, the spanwise equilibrium is lost and the dynamic stall vortex begins to exhibit strong three-dimensional features. In particular, the segments of the vortex near the mid-span become stronger than those on outboard sections. Evidence of this is forthcoming from the spanwise distribution of pressure at 17% of chord presented in Fig. 7. Here, despite a noticeable change in the pressure coefficient gradient across the span at point 1, the increased suction is most severe near the mid-span but, interestingly, it is also most short-lived.

At the same time as the increase in strength at the mid-span, the weaker segments of the vortex near the tip are forced downwards towards the surface by the tip vortices. The combined influence of these two effects apparently causes the central section of the vortex to lift from the surface, thus forming the so-called 'omega' structure. As these central portions lift away, the localised suction produced by them diminishes. This is apparent near the mid-chord in Fig. 4a, but is more graphically illustrated in Fig. 7. where the progressive chordwise diminution of the mid-span suction effect is clearly evident. In fact, by 83% of chord no build-up in suction can be detected at the mid-span. The expected rise in Cn due to the additional vortex lift is, therefore, also short lived and, as may be observed in Fig. 3., bears little resemblance to the 2-D data. Conversely, the suction produced by the vertical legs of the 'omega' vortex grows as both their strength and proximity to the wing surface increases. By 83% of chord, the pressure drop due to them (position 5) is substantial. This is also responsible for the more substantial rise in Cn shown in Fig. 5 at the 68% of span location.

Another important feature of Fig. 7, is the spanwise variation in vortex convection as witnessed by the pressure responses. It appears, from the data, that the mid-span segments move downstream faster than those outboard. This has been previously observed in flow visualisation studies and probably arises from the increased exposure of the raised section of the vortex to the freestream.

Throughout the build-up of the dynamic stall vortex, there is a corresponding increase in the strength of the tip vortices. In addition to the downwash from them, these vortices produce the localised suction identified in Fig. 7 on aft portions near the wing tips. As the dynamic stall vortex progresses downstream, it establishes connectivity with the tip vortices in a manner similar to that described by Horner[23]. It is, however, interesting to note, from the 83% of chord case in Fig. 7, that the tip vortex system collapses prior to the convection of the 'omega' vortex from the trailing edge. In fact, the strength of the tip vortices appears to be dominated by the growth and subsequent decay of leading edge suction.

With the convection of the 'omega' vortex from the trailing edge of the wing, secondary, Strouhal type, vortex shedding is initiated. Limited evidence of this is visible in Fig. 7 at 17% of chord (position 2) but, by 37%

the phenomenon has developed and leaves a clear imprint on the pressure distribution at position 4. Rapid convection of this vortex system away from the surface diminishes its effect at 83% of chord.

As the smoke flow images of Fig. 10 show, many of the basic features of the rectangular wing flowfield can also be identified in the swept tip wing case. On this wing, however, the extent of the tip vortex system substantially modifies the wing pressure distribution and, hence, the development and subsequent convection of the dynamic stall vortex.

The Cn curve produced by the swept tip wing at 57% of span is similar in form to that of the rectangular wing but exhibits a less rapid growth, corresponding to the slightly lower effective aspect ratio. At 68% of span, Fig. 5, the initial development follows this trend but the build-up in Cn following vortex initiation is less pronounced. These observations are echoed in the corresponding chordwise pressure distributions presented in Figs. 4 and 6 which show much weaker suction features than in the rectangular case. All of these are consistent with a weaker vortex formation which is rapidly convected upwards away from the wing surface. Indeed, it is almost impossible to detect any coherent chordwise convection in the series of pressure coefficient plots presented in Fig. 8.

Unlike the dynamic stall vortex, the tip vortex system appears as a strong feature of the measured pressure coefficient traces. In Figure 8, the increase in suction due to this system is significant at both 17% and 37% of chord but less so at 83%. In this respect, the tip vortex is more akin to that of a delta wing leading-edge vortex than a classical tip trailing vortex such as that of the rectangular wing. As may be observed in Fig. 10, it also directly impinges on a larger portion of the upper surface of the wing.

Clearly, the swept wing tips modify the manner in which the tip vortices and the dynamic stall vortex interact. The dominant tip vortices limit Cn growth across the entire wing and are, thus, responsible for a lowering of the effective reduced pitch rate experienced by the wing. This, in turn, reduces the strength of the dynamic stall vortex which is both constrained towards the mid-span and pushed upwards more rapidly than that of the rectangular wing. So much so, in fact, that its convection beyond the mid chord is difficult to detect from the pressure data.

Conclusions

A new experimental facility has been established to investigate the dynamic stalling of finite wings. In this study, the facility has been used to measure unsteady surface pressure variations on a rectangular planform wing and a swept-tip wing of similar overall dimensions. The spatial and temporal resolution of the collected data is such that the effects of flow structures, only previously observed in low Reynolds number flow visualisation studies, can be identified at the higher test Reynolds numbers.

Pressure signals indicative of the formation of a classical dynamic stall vortex were observed on both wings. In each case, this vortex appeared to distort significantly under the influence of the tip vortex system, forming a so-called 'omega' vortex. The subsequent chordwise convection of this vortex system could be identified from the pressure data.

The main influence of the swept-tips was to apparently increase the significance of the tip vortices with respect to the dynamic stall vortex. This, in turn, enhanced the distortion of the dynamic stall vortex.

Acknowledgements

The work was carried out with funding from the Engineering & Physical Science Research Council, (Grant Ref. SERC GR/H48330) Westland Helicopters, Defence Research Agency and the University of Glasgow. The authors acknowledge with gratitude the help and support of their sponsors.

References

[1] Harper, P.W., Flanigan, R.E., 'The effect of change of angle of attack on the maximu lift of a small model', NACA TN-2061, 1950

[2] Moss,G.F., Murdin,P.W., ' Two dimensional low-speed tunnel tests on the NACA 0012 section including measurement made during pitch oscillations at the stall', RAE Technical Report CP No. 1145, 1968

[3] McCroskey,W.J, and Fisher, R.K. ' Detailed aerodynamic measurements on a model rotor in the blade stall regime', AIAA Journal, Vol. 17, No.1, pp 20-30, 1972.

[4] McAlister, K.W., Carr,L.W.,and McCroskey, W.J. ' Dynamic stall experiments on NACA0012 airfoil', NACA TP-1100, 1978

[5] Petot, J.J., ' Experimental and theoretical studies on helicopter blade tips at ONERA', 6th European Rotorcraft and Powered Lift Aircraft Forum, Bristol, 1980

[6] Wood,M.E., ' Results of oscillatory pitch and ramp tests on the NACA0012 blade section', ARA Memo No. 220, December, 1979

[7] Carta,F.O., ' Experimental investigation of the unsteady aerodynamic characteristics of a NACA 0012 airfoil', Res. Rep. M-1283-1, United Aircraft Corp., July,1960

[8] Young,W.H.,Jr,' Fluid mechanics mechanisms'. NASA -TM- 81956, March 1981

[9] Carr, L.W., 'Progress in analysis and prediction of dynamic stall', Journal of Aircraft, Vol. 25, No. 1., January 1988

[10] Lorber,R.F., Carta,F.O., 'Unsteady stall penetration experiments at high Reynolds number', AFOSR TR-87-1202, UTRC R87-956939-3, 1987

[11] Galbraith,R.A.McD, Gracey, M.W. and Leitch, E., 'Summary of pressure data for thirteen aerofoils on the University of Glasgow's aerofoil database', G.U. Aero Report: 9221, 1992.

[12] Green,R.B, Galbraith,R.A.McD, Niven,A.J.,' Measurements of the dynamic stall vortex convection speed', The Aeronautical Journal of The Royal Aeronautical Society, October 1992

[13] Beddoes,T.S., 'Representation of airfoil behaviour', AGARD Specialists Meeting on the Prediction of Aerodynamic Loads on Rotorcraft, AGARD CP-334, 1982, also Vertica, Vol. 7, (2)., 1983

[14] Leishman,J.G., Beddoes,T.S., ' A semi-empirical model for dynamic stall', Journal of The American Helicopter Society, July 1989

[15] Gangwani,S.T., ' Synthesised airfoil data method for prediction of dynamic stall and unsteady airfoils', Proceedings of the 39th Annual Forum of the America Helicopter Society, 1983, also Vertica, Vol. 8, 1984

[16] Tran,C.T., Petot,D., ' Semi-empirical model for the dynamic stall of airfoils in view of the application to the calculation of responses', ONERA T.P. 103-1980.

[17] Beddoes,T.S., ' A 3-D separation model for arbitrary planforms', 47th Annual Forum of the American Helicopter Society, Phoenix, Arizona, May 1991

[18] Gad-el-Hak, M., Ho., C-M., 'The pitching delta wing', AIAA Journal, Vol. 23, No. 11, Nov. 1985

[19] Thompson, S.A., Batill, S.M., Nelson, R.C., 'Delta wing surface pressures for high angle of attack maneuvres', AIAA Atmospheric Flight Mechanics Conference, Oregon, 1990

[20] Ashworth, J., Huyer, S., Luttges, M., 'Comparisons of unsteady flow fields about straight and swept wings using flow visualization and hot-wire anemometry', AIAA 19th Fluid Dynamics, Plasma Dynamics and Lasers Conference, Hawaii, 1987

[21] Ashworth, J., Crisler, W., Luttges, M., 'Vortex flows created by sinusoidal oscillation of three-dimensional wings', AIAA 7th Applied Aerodynamics Conference, Seattle, 1989

[22] Freymuth, P., 'Visualizing the connectivity of vortex systems for pitching wings.', Journal of Fluids Engineering, Vol. 111, pp217-220, June 1989

[23] Horner,M.B., Addington, G.A., Young III, J.W. and Luttges, M.W., 'Controlled Three-Dimensionality in Unsteady Separation Flows about a Sinusoidally Oscillating Flat Plate', AIAA- 90-0689, Jan. 1990

[24] Piziall, R.A., ' 2-D and 3-D Oscillating Wing Aerodynamics for a Range of Angles of Attack Including Stall', NASA-TM-4632, September 1994

[25] Jiang, D., Coton, F. N., Galbraith, R.A.McD., Gilmour, R.,' Collected data for tests on a NACA 0015 section rectangular wing (aspect ratio 3)', Vols. 1 - 8, G.U. Aero. Repts 9515 - 9522, 1995

[26] Galbraith, R. A. McD., Coton, F. N., Jiang, D., Gilmour, R., 'Preliminary results from a three-dimensional dynamic stall experiment of a finite wing', 21st European Rotorcraft Forum, St. Petersburg, Russia, 1995

[27] Moir, S., Coton, F.N., 'An examination of the dynamic stalling of two wing planforms', G.U. Aero. Report 9526, 1995

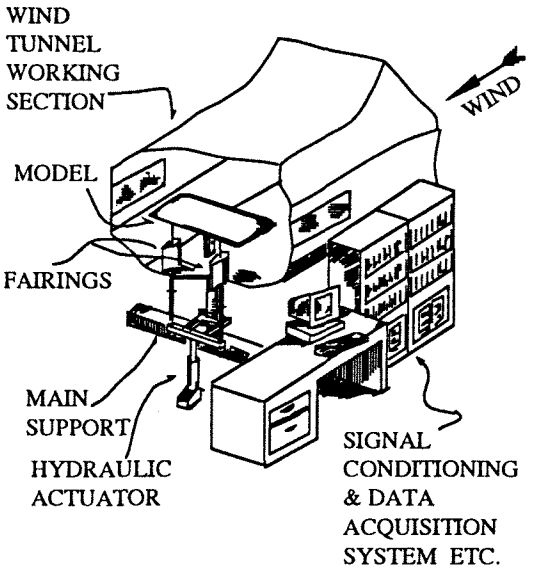

FIGURE 1. Test set-up

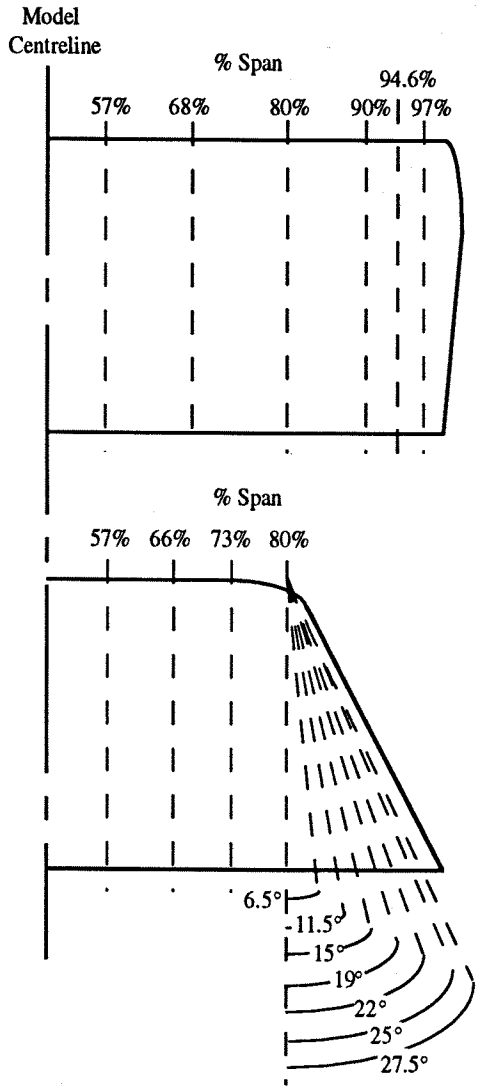

FIGURE 2. Location of main transducer arrays

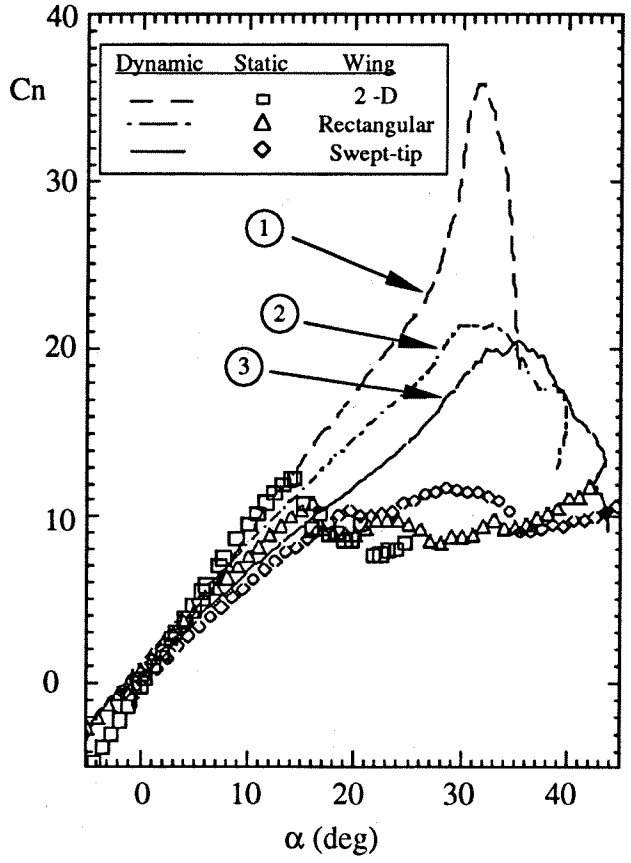

FIGURE 3. Normal force coefficient versus angle of attack at 57% of span in steady and unsteady flow. ($Re = 1.5 \times 10^6$)

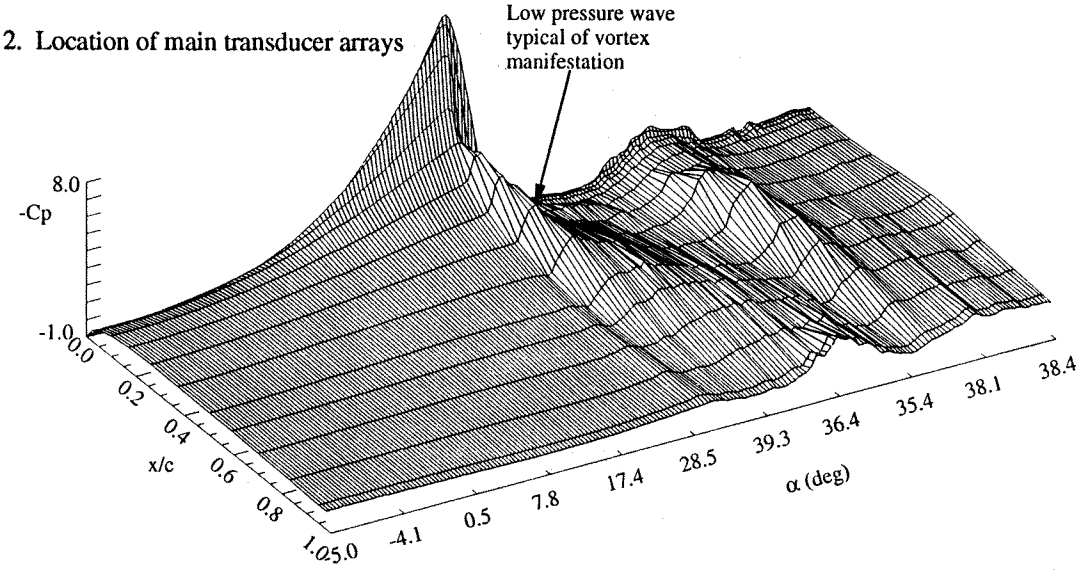

FIGURE 4a. Variation of chordwise pressure with angle of attack at 57% of span on rectangular wing

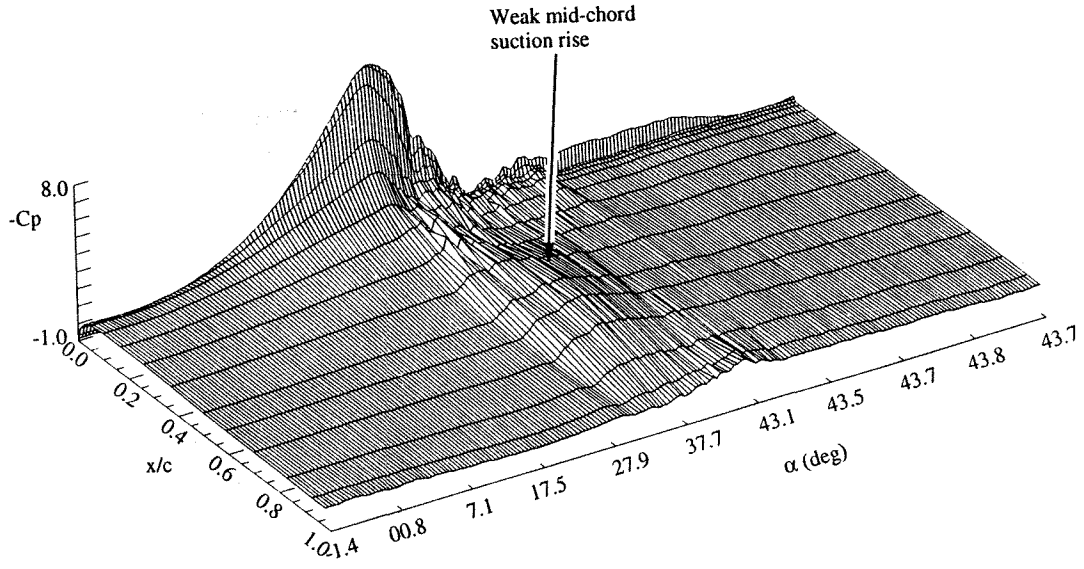

FIGURE 4b Variation of chordwise pressure with angle of attack at 57% of span on swept-tip wing

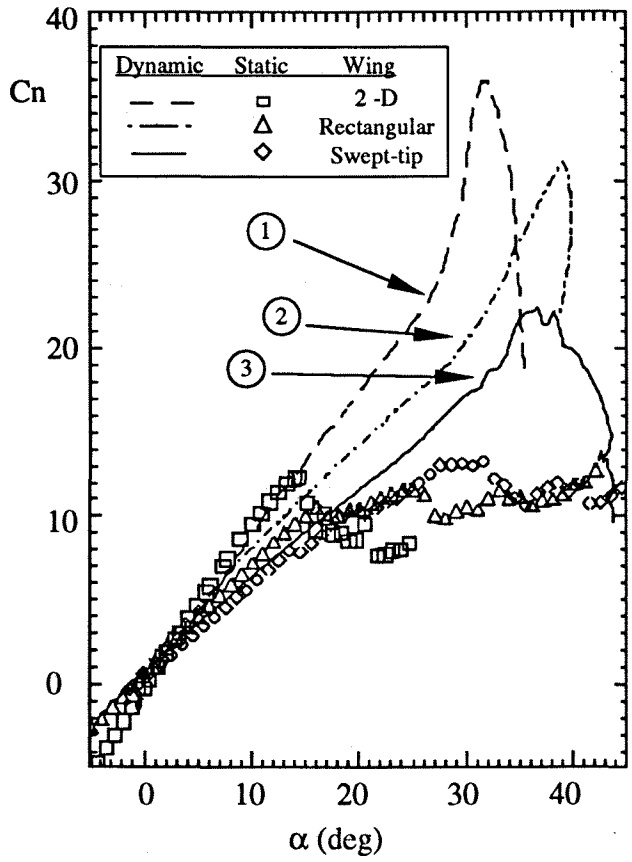

FIGURE 5. Normal force coefficient versus angle of attack between 66% and 68% of span in steady and unsteady flow. (Re = 1.5 x 10^6)

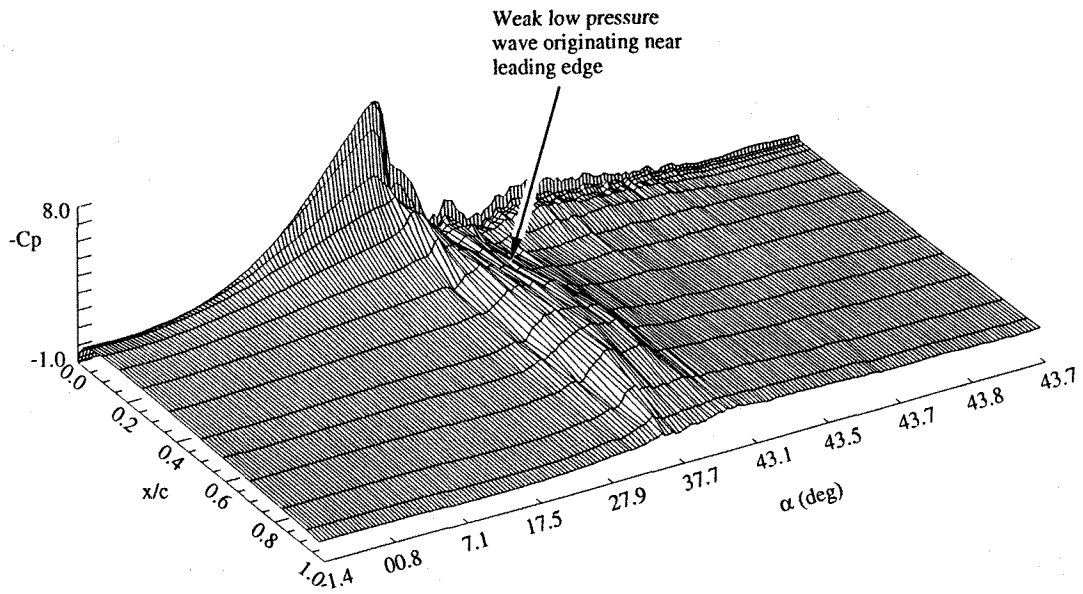

FIGURE 6a Variation of chordwise pressure with angle of attack at 68% of span on rectangular wing

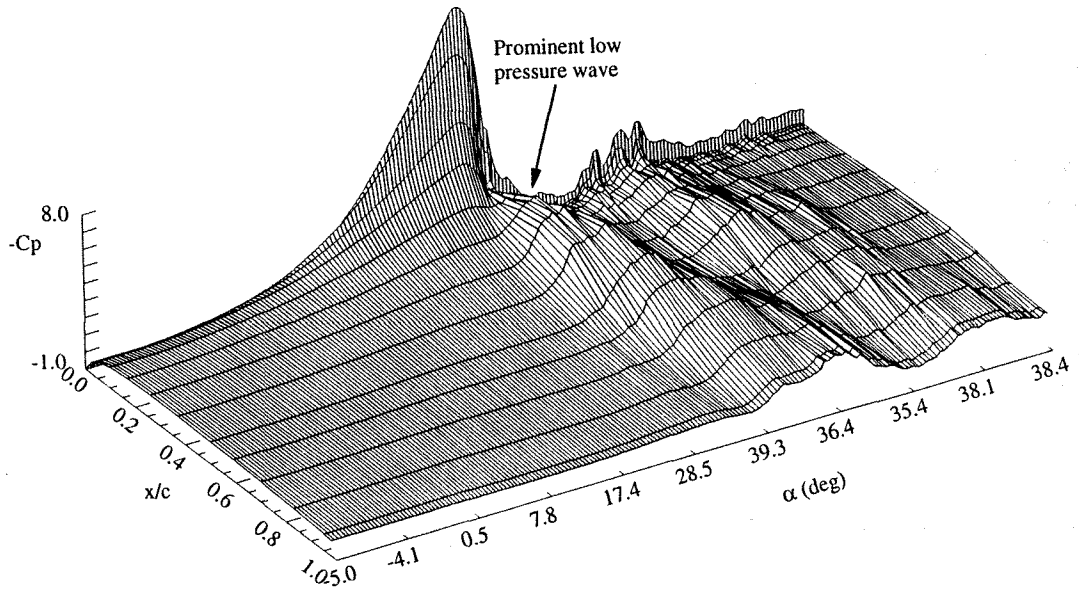

FIGURE 6b Variation of chordwise pressure with angle of attack at 66% of span on swept-tip wing

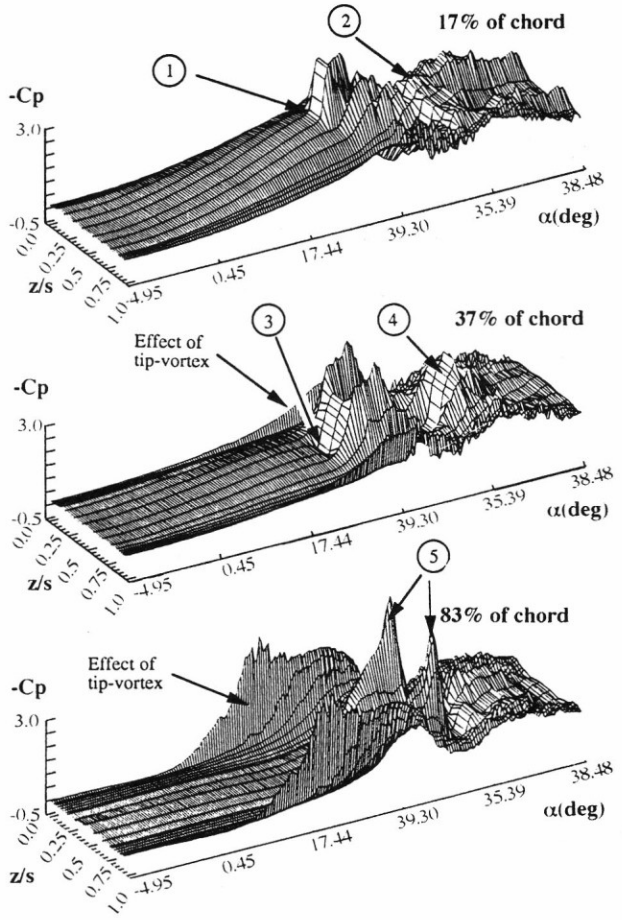

FIGURE 7. Spanwise pressure distribution at three chordal locations on the rectangular wing against angle of attack

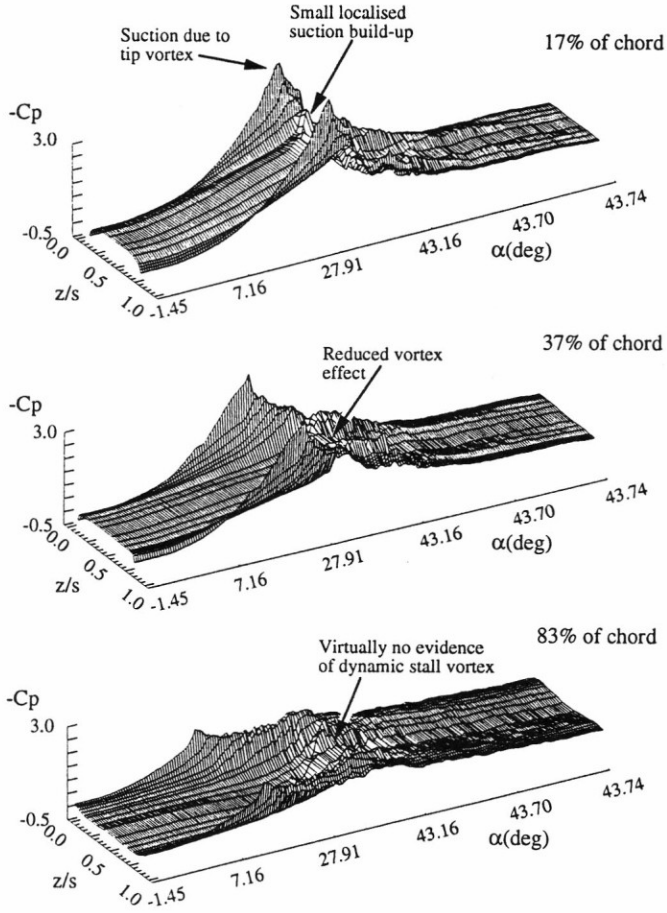

FIGURE 8. Spanwise pressure distribution at three chordal locations on the rectangular wing against angle of attack

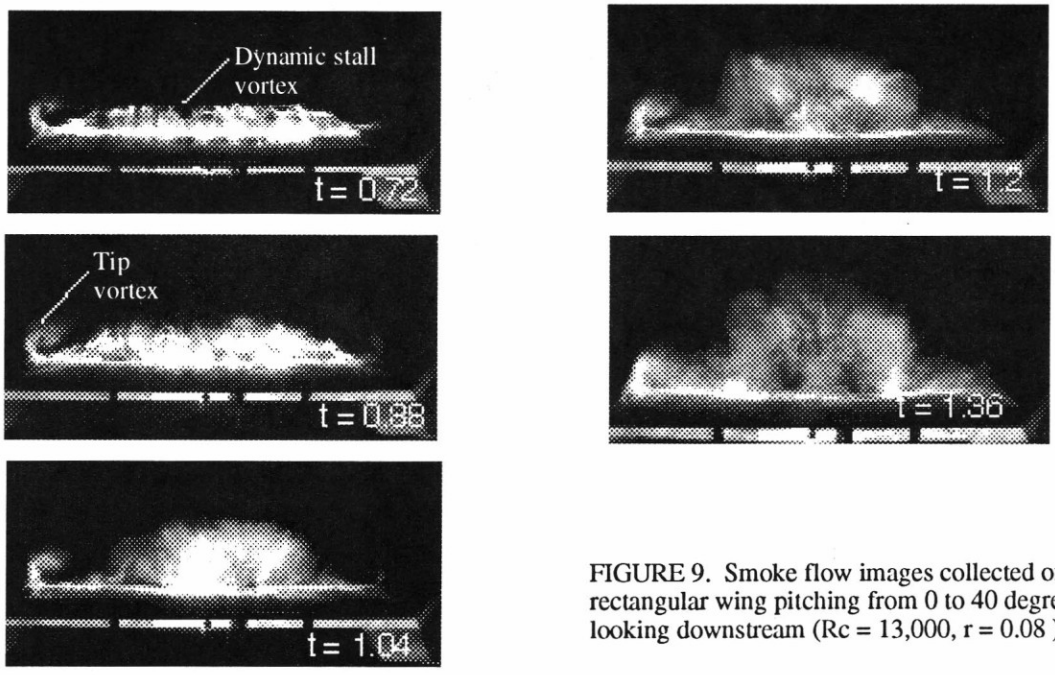

FIGURE 9. Smoke flow images collected on a rectangular wing pitching from 0 to 40 degrees, view looking downstream (Rc = 13,000, r = 0.08)

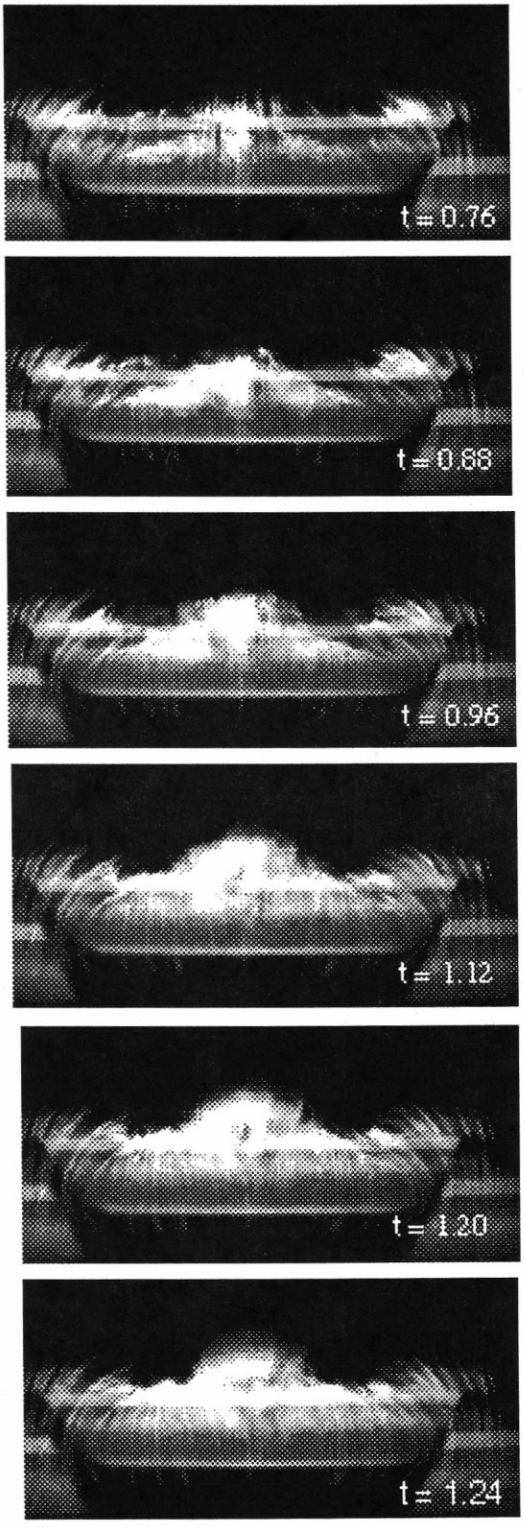

FIGURE 10. Smoke flow images collected on a swept-tip wing pitching from 0 to 40 degrees, view looking downstream (Rc = 13,000, r = 0.08)

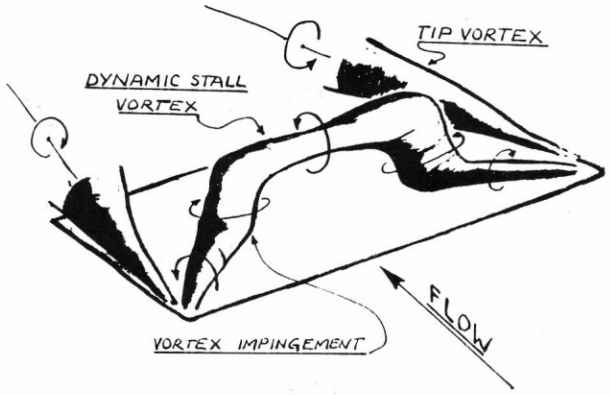

FIGURE 11a. Sketch of the 'omega' vortex system

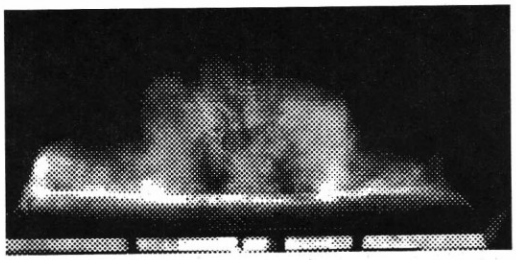

FIGURE 11b. Manifestation of the 'omega' vortex on the upper surface of the pitching rectangular wing